CHAPTER 1

INTRODUCTION

1.1 Introduction

Looking back at the cytological study and improvement of molecular techniques in recent years, scientist now are able to understand cytoskeletal elements in bacterial cell (Carballi-do-Lopez and Errington, 2003) that lead into the third cytoskeletal element that is intermediate filaments whereby the first and second are tubulin and actin.

Despite of its micro size, bacteria is a unique creation on earth that giving scientist abundant of research to study including the cytokinesis process. It is known that in *Escherichia coli*, the cell divides into two at midcell to produce daughter cells. The symmetrically division of these rod shape bacteria are driven by protein-protein interactions.

1.2 Min System

Min system is one of the examples of self-organization in *E.coli*. The role of Min System in Z ring formation is known to prevent constriction at cell poles. How the proteins in Min system react with each other? It is by oscillation created from the movement of Min proteins from pole to pole with exact reaction-diffusion rate.

The oscillation however, requires a few components such as MinC, MinD, MinE and ATP. Thus the information on Min oscillation make possible for researchers to investigate *in silico* simulation to model the key features of the system.

1.2.1 MinC

The role of MinC in Min system has been described as an inhibitor that antagonizes the Z ring formation. MinC in a normal condition exist as a dimer in the cell. It contains two domain terminals, N-terminal and C-terminal. The N-terminal is responsible in two ways, *in vivo* and *in vitro*. In *in vivo*, the N-terminal domain inhibits the cell division and in *in vitro*, it antagonizes the assembly of FtsZ filaments. The C-terminal domain instead, responsible in dimerization and interaction with MinD (Lutkenhaus J., 2007).

Although MinC is the effector for the Min system, it is relatively weak inhibitor without the presence of MinD. By recruiting the MinC to the membrane, MinD activates the function of MinC almost ~25 to 50 fold (de Boer P.A., Crossley R.E., Rothfield L.I., 1992). MinC dependency on MinD activation is not sufficient to increase the inhibition activity; it also acquired affinity for septal component.

1.2.2 MinD

MinD is an ATPase. The function of MTS presence at the C-terminal end of the protein is to anchor MinD to membrane. In addition, MinD also reacts with phospholipid to activate the MinD ATPase. A study from Hu Z., Saez C. and Lutkenhaus J., (2002) resulted in proving that MinD also recruits MinC to bicelles.

MinD ATPase requires MinE in order to stimulate it ~10 folds faster, however it also required MinD to bound with membrane surface to start the stimulation (Hu Z. and Lutkenhaus J., 2001).

1.2.3 MinE

The structure that has been described by King G.F., Shih Y.L., Maciejewski M.W., Bains N.P., Pan B., *et. al*. (2000) for MinE is that this protein forms a dimer with 88 amino acids residues. Generally, MinE responsible in restricting the MinC/MinD complex to cell poles that inhibits the formation of FtsZ at this area. The specific function of MinE depends on the N-terminal and C-terminal.

The N-terminal MinE consists of anti MinC/MinD activity that suppresses the inhibition activity without topological specificity. When binds to MinD, MinE will stimulate the ATPase activity of MinD, thus convert it to inactive form.

The C-terminal domain responsible in MinC/MinD complex restriction activity. The structure of the domain makes possible for MinE dimerization (King G.F., Shih Y.L., Maciejewski M.W., Bains N.P., Pan B., *et. al*., 2000). However, recent study indicated that N-terminal interact with C-terminal domain, suggesting that both domains are not depending on each other to complete the Min system (Ramos D., Ducat T., Cheng J., Eng N.F., Dillon J.A., Goto N.K., 2006).

1.3 MinDE System Model

Previous model of the Min system reported that MinC/MinD complex is evenly distributed on the membrane to inhibit Z ring formation anywhere in the cell. With the presence of MinE, anti MinC/MinD complex, it restricting the complex to the poles thus prevent mini cell formation by allowing the Z ring to form at the midcell.

Figure 1 shows the MinDE system model that was based on the concept that when MinE is absent, the sensitivity of MinC/MinD complex is equal within the cellular location. Thus, the restriction of MinC/MinD complex to the poles will not occur without MinE.

Equal distribution of MinC/MinD within the cellular location results in deformation of FtsZ and led to cell elongation where else minicell is the results of imbalance of MinC/MinD distribution in the cell.

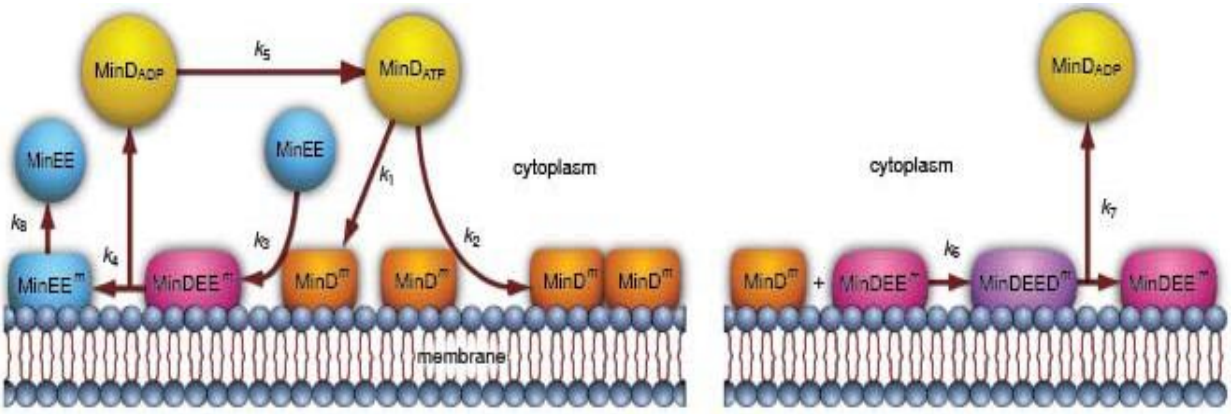

Figure 1 MinDE System Model. This model is taken from Arjunan S.N.V, (2009).

The model consists of three main species of Min, MinC, MinD and MinE. When $MinD_{ATP}$ in the cytoplasm binds to the membrane with the help of lipids in the cytoplasm, it will produce membrane MinD ($MinD^m$). The membrane MinD will then associates back with cytocolic $MinD_{ATP}$ to produce another 2 molecules of $MinD^m$. With the presence of MinE dimer (represented as MinEE in the figure), $MinD^m$ recruits the dimer and produces MinD/MinE complex or represented as $MinDEE^m$ in the figure. In this complex, MinE stimulates the ATPase function to release the MinD back to the cytoplasm. This is where the MinD disassociates from the membrane but leaving the MinE remains bound to the membrane ($MinEE^m$). The membrane $MinEE^m$ then releases back to the cytoplasm. The disassociated MinD is then undergo phosphorylation in the cytoplasm to start back the cycle for MinDE oscillation.

According to S.N.V Arjunan and M. Tomita (2009), there are eight series of reactions altogether to complete the MinDE system. The reactions can be described as follows;

i) $MinD_{ATP} \xrightarrow{k_1} MinD^m$, (1)

ii) $MinD^m + MinD_{ATP} \xrightarrow{k_2} 2MinD^m$, (2)

iii) $MinD^m + MinEE \xrightarrow{k_3} MinDEE^m$, (3)

iv) $MinDEE^m \xrightarrow{k_4} MinD_{ADP} + MinEE^m$, (4)

v) $MinD_{ADP} \xrightarrow{k_5} MinD_{ATP}$, (5)

vi) $MinD^m + MinDEE^m \xrightarrow{k_6} MinDEED^m$, (6)

vii) $MinDEED^m \xrightarrow{k_7} MinD_{ADP} + MinDEE^m$, (7)

viii) $MinEE^m \xrightarrow{k_8} MinEE$. (8)

Previous scientist experimentally identified the parameter values for the simulation. Table 1 list all the parameters related to the simulation of MinDE system.

Parameter	Value	Source
k1	0.022 μm s^{-1}	Fitted
k2	0.03 μm^3 s^{-1}	Fitted
k3	0.5 μm^3 s^{-1}	Fitted
k4	1 s^{-1}	Fitted
k5	5 s^{-1}	(Meacci *et. al* , 2006)
k6	5000 μm^3 s^{-1}	Fitted
k7	1 s^{-1}	Fitted
k8	0.83 s^{-1}	Fitted

Parameter	Value	Source
$D_{MinD_{ATP}}$, $D_{MinD_{ADP}}$	16 μm^2 s^{-1}	(Meacci *et. al*., 2006)
D_{MinEE}	10 μm^2 s^{-1}	(Meacci *et. al*., 2006)
D^m	0.02 μm^2 s^{-1}	Approximated
Cell volume	3.27 μm^3	Approximated
Cell radius	0.5 μm	Approximated
Cell length	4.5 μm	Approximated
r_v	10 nm	Approximated
MinD$^{\#}$	2000 molecules	(Shih *et. al*., 2002)
MinE$^{\#}$	1400 molecules	(Shih *et. al*., 2002)

Table 1 Simulation parameters of the MinDE model.

This table taken from Arjunan S.N.V. and Tomita M. (2009)

1.4 FtsZ

The cytokinesis process in bacteria is associated with the formation of Z ring at the midcell. The first protein that localized in Z ring was filamenting temperature sensitive Z, also known as FtsZ (Bi. E., Lutkenhaus J., 1991). This cytokinetic machinery in bacteria specifically in *E.coli* is driven by positive and negative regulators of Z ring. The balance of positive and negative role of these regulators help in stability and dynamicity of Z ring, thus complete the cell division process.

The positive regulator helps to decrease the concentration of Z ring and enhance the capacity of FtsZ to stabilize divisome complex. Proteins that falls under positive regulators are FtsA, ZipA, Zap A and SepF. Antagonistically, the negative regulator increase the critical concentration of Z ring, thus prevent septum formation at inappropriate location and odd cell division stage. There are Min System (MinCDE), SulA, EzrA and NO (nucloid occlusion). Here, we will only discuss on positive and negative regulator that are involved in Z ring formation in *Escherichia coli*

In *E.coli*, formation of Z ring starts right after chromosome replication and segregation into nucleoids took place (Dajkovic A., Lutkenhaus J., 2006). A normal symmetrical two daughter cells will have the Z ring formation at mid cell to prevent mini cell production. The formation of Z ring at the mid cell is driven by a protein system that prevents Z ring or more precisely FtsZ to form anywhere else in the cell. Constriction of Z ring then occurs to complete the cell division. The role of FtsZ is to act as a scaffold (David W Adams and Jeff Errington, 2009) to form polymers of Z ring in the middle of the cell. The ability of FtsZ to bind with GTP enables filamentation to occur *in vivo.*

However, in recent year (2010), Shen B. and Lutkenhaus J. has successfully proved by laboratory experiment that without the presence of MinE, there are differences in MinC/MinD sensitivity between polar and internal Z ring in *E.coli*. They used the FtsX-I374V strain and found out that with lack of MinE in that particular population, there were less production of minicell. It shows that MinC/MinD have the potential to recruit themselves to the poles even without the help of MinE. It was predicted that the behavior of MinC/MinD is most likely because of the rod shape of the *E.coli* itself. The high curvature of the poles might increase the binding probability of MinC/MinD at that area and thus inhibits formation of FtsZ.

In this *in-silico* research, we try to simulate the model by; first, discarding the MinE from the original model, to imitate the result that has been discovered by laboratory experiment indicated that polar Z rings are more susceptible to MinC/MinD than internal Z rings even when MinE is absent. Second, modify the parameter values of all the reaction-diffusion rate involved to adapt with the new model that bypassing MinE. Finally, the goal is to observe the behavior of MinD with all the parameter changes.

75 changes has been made to three conditions; 1) changes in initial values of $MinD_{ATP}$, $MinD_{ADP}$ and $MinD^{m}$ molecule, 2) changes in coefficient (D) of $MinD_{ATP}$, $MinD_{ADP}$ and $MinD^{m}$ and 3) changes in reaction rate of k1, k2, k3 and k4. The results suggested that there are several conditions that nearly restrict all the membrane MinD molecules to the poles. However, there were no oscillation occurs in any of the condition changes. We assumed that the binding probability of MinD to the membrane is still low and further modification need to be done in order to complete the new system that bypassing MinE.

CHAPTER 2

LITERATURE REVIEW

2.1 Literature Review

Simulation on bacterial divisome has been done using computational methods that are very useful to biologists to evaluate their predictions in both qualitative and quantitative way. Another important thing in simulation study is that it can provide mechanistic insights (Treanor and Batista, 2007; Clarke and Liu, 2008; Neves and Iyenger, 2009).

Though it has been experimentally approved that MinC / MinD is more preferred to localized at poles with different polar and non-polar sensitivity without the present of MinE, there is no evidence on computational model to simulate and evaluate the results that give rise to this *in silico* research.

A lattice based Monte Carlo method called Spatiocyte that support reaction diffusion (RD) in volume and surface compartments at single molecule is used to model and analyzed the result (Arjunan S.N.V, Tomita M., 2009). There are many examples of spatial modeling methods such as Virtual Cell (Schaff *et. al*., 2001), MesoRD (Elf and Ehrenberg, 2004; Hattne *et. al.,* 2005), Smoldyn (Andrews and Bray, 2004), SmartCell (Ander *et. al.,* 2004), GFRD (van Zon and ten Wolde, 2005), GMP (Rodriguez *et. al*., 2006), Cel++ (Sanford *et. al.,* 2006), CyberCell (Ridgway *et. al*., 2008), GridCell (Boulianne *et. al*., 2008), STEPS (Will and Schutter, 2009) and eGFRD (Takahashi *et. al.,* 20009).

The major different between Spatiocyte with other spatial modeling methods is the temporal evolution, which is the simulation time-stepping scheme that is used in Spatiocyte. It is based on the hybrid-time and event-driven simulation method. Another special feature

that is built in this method is the ability to simulate in multicompartmental environment to simulate the reactions in cytoplasm and membrane area in *E.coli*.

A few critical points that has to be taken into consideration to begin the Spaciocyte computational simulation are 1) multicomparmental simulation space, 2) diffusion; diffusion-independent reaction, diffusion-influenced reactions; irreversible and reversible reaction, 3) hybrid time- and event-driven simulation, 3) simulating fluorescence microscopy images, 4) modeling the ring (Arjunan S.N.V, Tomita M., 2009).

2.2 Multicompartmental simulation space

We understand that there are different kinds of reaction take part in different environment in bacteria cell. Take *E.coli* as an example, protein molecules can involve in reaction that either, mobile and distributed evenly in the environment or static and localized at specific area. In spatiocyte, there are a few types of reaction, first- and second- order reaction with homogenously (HD) or non-homogenously (non-HD) species. This multicompartmental space is created based on the understanding that at the surface compartment the lipid molecules are immobile while at the molecular scale, ATPs are freely distributed within the cytoplasm space. The HD and non-HD species is referred to the mobility of the molecule itself. If the molecule is mobile and distributed evenly within the compartment, it is considered as HD molecule (Arjunan S.N.V, Tomita M., 2009).

2.3 Diffusion

2.3.1 Diffusion-independent reactions

Diffusion–independent reactions in the Spatiocyte represented as Next Reaction method (NR) (Gibson and Bruck, 2000). Basically, it follows the first order reaction

A $\xrightarrow{k_A}$ product(s), where the product(s) comprising diffusing, immobile or HD species. The NR method is using a Gillespie algorithm (Gillespie 1976;1977), algorithm that can simulate reactions efficiently and accurately.

2.3.2 Diffusion-influenced reactions

Diffusion-influenced reactions is a condition where in a second order reaction, A + B $\xrightarrow{k_A}$ product(s), involve a diffusing and immobile reactant and two diffusing reactants (Arjunan S.N.V, Tomita M., 2009). The model is based on Collins and Kimball approach (Collins and Kimball, 1949) using spatially discretized version.

2.4 Hybrid time- and event-driven simulation

Due to the requirement to capture the real-time system in Spatiocyte simulation, a hybrid of time- and event-driven is an ideal process to implement. In order to run a simulation of complex time- and event-driven process, a powerful and suitable algorithm is required; therefore, a multi-timescale algorithm was adopted for this E-cell System (Takahashi *et. al*., 2004). The integration of different types of algorithm is capable to manage both diffusion for time-driven process and diffusion-independent reactions for event-driven process (Arjunan S.N.V, Tomita M., 2009).

2.5 Simulating fluorescence microscopy images

Currently, fluorescence labeling is known to be the option for visualization of molecules localization in spatial modeling (Resch-Genger *et. al*., 2008; Fernández-Suárez and Ting, 2008; Ji *et. al*., 2008, Huang *et. al*., 2009). The drawbacks of using fluorescence microscopy are first, low resolution resulted in low quality images, second, the differences

in time exposure, even a millisecond interval might lose the chance to capture the position of diffusing molecules.

Based on the drawbacks, a computational method for spatial visualization has been developed to simulate the microscopy images. A program called OpenGL is used to display the simulated trajectory. The RGBA mode (red, green, blue and alpha) represents the molecules involved in the systems where else, the black background represents the unlit microscopy space (Arjunan S.N.V, Tomita M., 2009).

2.6 Modeling the ring

It is based on the experimental result derived from FtsZ-I34V strain, which shows that cells with lack of MinE, clearly indicates that MinC/MinD eliminates polar Z rings without inhibiting the midcell ones (Shen B., Lutkenhaus J., 2010).

Previous study that proves MinE regulates the oscillation of MinC/MinD to the poles to produce E ring focused at the MinE properties, domains at two terminal, C-terminal and N-terminal (Arjunan S.N.V, Tomita M., 2009). Two assumptions from the study; firstly, as suggested by Ma *et. al*., (2003), binding domain of MinE N-terminal is only exposed upon binding with MinD on the membrane. Secondly, the MinE can only begin to transiently attach to the membrane independently of MinD when it is in dimer form with the membrane binding domains at both N-terminals exposed (Arjunan S.N.V, Tomita M., 2009).

However, in the new suggested model, the MinE properties are no longer a critical point for the FtsZ inhibition at the poles. In facts, the model is bypassing the MinE for spatial regulation of cytokinesis by MinC/MinD. The strain that was induces with 1mM concentration of IPTG (isopropyl-β-D-thiogalactopyranoside) produce wild-type

morphology (Shen B., Lutkenhaus J., 2010). In this population, cell division occurs at midcell and that polar Z ring is undetectable by immunostaining (Shen B., Lutkenhaus J., 2010).

2.7 MinC/MinD System Model Bypassing MinE

Laboratory experiment in the FtsZ-I374V strain give evidence that MinC/MinD complex has a different sensitivity between polar and non-polar Z ring even when there is no MinE (Shen B., Lutkenhaus J., 2010). The disruption of interaction between FtsZ and MinC domains appears to function normally without any minicells production in the studied FtsZ mutant's strains, BSZ374 and BSZ280D.

CHAPTER 3

MATERIAL AND METHODOLOGY

3.1 Material and Method

Modeling reaction and diffusion of MinD in *Escherichia coli* was done using E-Cell Spatiocyte version 3.2.1 in Ubuntu Linux version 11.04 (Natty Narwhal) operating system. Three steps that were involved in this *in silico* research are 1) modification of a new model for MinC/MinD bypassing MinE, 2) identification of a series of reaction that based from MinDE system (Arjunan S.N.V., Tomita M., 2009), 3) optimization of diffusion-reaction based for new model MinC/MinD system

3.2 Modification of a new model for Minc/MinD bypassing MinE

It is known that in the current model for the Min system, the MinC/MinD division inhibitory complex is evenly distributed on the membrane and can disrupt Z rings anywhere in the cell, thus the protein that responsible to spatially regulates MinC/MinD to the cell poles is MinE. This phenomenon created a midcell restriction as the formation of Z ring restricted only at the midcell. Assumption arise from that study is Z rings formed at different cellular locations have equal sensitivity between MinC/MinD in the absence of MinE. In the latest research by Shen B. and Lutkenhaus J. (2010), they successfully proved that although without the presence of MinE, there is a differences in MinC/MinD sensitivity between polar and nonpolar Z rings.

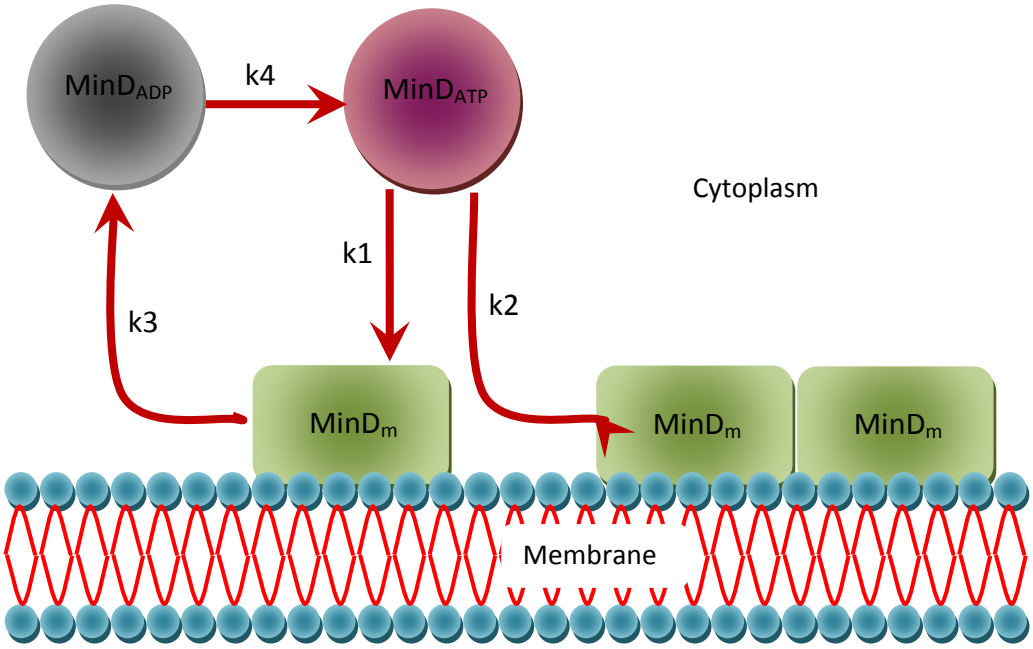

Figure 2 Suggested Model of MinC/MinD bypassing MinE

Figure 2 shows the suggested model of MinC/MinD bypassing MinE. Similar to the established model of MinDE system, it started with association of $MinD_{ATP}$ with lipid in the cytoplasm that produces MinD membrane molecules. A reverse back reaction of membrane MinD molecules with cytosolic $MinD_{ATP}$ produces another two molecules of membrane MinD. In the original model, the separated membrane MinD that produced in a dimer form will recruits cytosilic MinE that also in a dimer form, to the membrane, but as we discarded MinE from the model, the separated membrane MinD will disassociate and self stimulate the ATPase function to release back the MinD to cytoplasm to become $MinD_{ADP}$. As it is freely moved in the cytoplasm, phosphorylation of the ADP took part that changes it back to phosphorylated $MinD_{ATP}$.

3.3 Identification of reaction

To start the new model of bypassing MinE in the Z ring formation, a series of reactions need to be identified first. As been discussed in the previous section, the proposed reactions of the model are as follows;

i) Association of MinD to the membrane,

$$MinD_{ATP} \xrightarrow{k_1} MinD^m \qquad (1)$$

ii) Second association of MinD to the membrane,

$$MinD^m + MinD_{ATP} \xrightarrow{k_2} 2MinD^m \qquad (2)$$

iii) Disassociation of MinD to the cytoplasm,

$$MinD^m \xrightarrow{k_3} MinD_{ADP} \qquad (3)$$

iv) ADP dephosphorylation,

$$MinD_{ADP} \xrightarrow{k_4} MinD_{ATP} \qquad (4)$$

Note that reaction *(1), (2)* and *(4)* are adapted from the well known MinDE model by Huang et. al. (2003) and Arjunan S.N.V, Tomita M., (2009). However, in reaction *(3)*, instead of MinE in the $MinDEE^m$ complex that stimulates MinD ATPase function based on MinDE system, we assumed that the ATPase is self stimulate to release the MinD to the cytoplasm.

3.4 Optimization of diffusion-reaction based for new model MinC/MinD system

To further complete the model, the diffusion and reaction rate needs to be optimized in order to achieve localization of MinD membrane to the poles. Optimization of the diffusion and reaction rate involved parameters such as, initial value of $MinD_{ATP}$ molecule, initial value of $MinD_{ADP}$ molecule, initial value of $MinD^m$ molecule, diffusion coefficient of

$MinD_{ATP}$, diffusion coefficient of $MinD_{ADP}$, diffusion coefficient of $MinD^{m}$, reaction rate k1, k2, k3 and k4.

3.4.1 Modification of the initial value of $MinD_{ATP}$, $MinD_{ADP}$ and $MinD^{m}$ molecules

In was reported in the previous research that initial potential of the molecules whether in the cytoplasm or in the membrane showed no changes in the oscillation of MinD (Arjunan S.N.V, Tomita M., 2009). To prove that, here, we changed the potential initial value of $MinD_{ATP}$ to see the effect. Modification was made based on the increment of the total number of molecules in the cell equal to 2000, 4000, 8000 and 16000 molecules.

Molecule's initial value	$MinD_{ATP}$ molecule	$MinD_{ADP}$ molecule	$MinD^{m}$ molecule
Initial value from established model	2000	0	0
Increment in the initial $MinD_{ATP}$ molecule (2X)	4000	0	0
Increment in the initial $MinD_{ATP}$ molecule (4X)	8000	0	0
Increment in the initial $MinD_{ATP}$ molecule (8X)	16000	0	0
Increment in the initial $MinD_{ADP}$ molecule	0	2000	0
Increment in the initial $MinD_{ADP}$ molecule (2X)	0	4000	0
Increment in the initial $MinD_{ADP}$ molecule (4X)	0	8000	0
Increment in the initial $MinD_{ADP}$ molecule (8X)	0	16000	0
Increment in the initial $MinD^{m}$ molecule	0	0	2000
Increment in the initial $MinD^{m}$ molecule (2X)	0	0	4000
Increment in the initial $MinD^{m}$ molecule (4X)	0	0	8000
Increment in the initial $MinD^{m}$ molecule (8X)	0	0	16000

Table 2 Initial value of $MinD_{ATP}$, $MinD_{ADP}$ and $MinD^{m}$ molecule modification

3.4.2 Modification of the Diffusion Coefficient of $MinD_{ATP}$, $MinD_{ADP}$ and $MinD^m$

The Diffusion coefficient of $MinD_{ATP}$, $MinD_{ADP}$ and $MinD^m$ were simulated according to Table 3. Modification was made based on increment of two folds (2X), four folds (4X) and eight folds (8X).

Diffusion Coefficient	$MinD_{ATP}$	$MinD_{ADP}$	$MinD^m$
D value from established model	16 $\mu m^2 s^{-1}$	16 $\mu m^2 s^{-1}$	0.02 $\mu m^2 s^{-1}$
Increment in the D $MinD_{ATP}$ (2X)	32 $\mu m^2 s^{-1}$	16 $\mu m^2 s^{-1}$	0.02 $\mu m^2 s^{-1}$
Increment in the D $MinD_{ADP}$ (2X)	16 $\mu m^2 s^{-1}$	32 $\mu m^2 s^{-1}$	0.02 $\mu m^2 s^{-1}$
Increment in the D $MinD^m$ (2X)	16 $\mu m^2 s^{-1}$	16 $\mu m^2 s^{-1}$	0.04 $\mu m^2 s^{-1}$
Increment in the D $MinD_{ATP}$ (4X)	64 $\mu m^2 s^{-1}$	16 $\mu m^2 s^{-1}$	0.02 $\mu m^2 s^{-1}$
Increment in the D $MinD_{ADP}$ (4X)	16 $\mu m^2 s^{-1}$	64 $\mu m^2 s^{-1}$	0.02 $\mu m^2 s^{-1}$
Increment in the D $MinD^m$ (4X)	16 $\mu m^2 s^{-1}$	16 $\mu m^2 s^{-1}$	0.08 $\mu m^2 s^{-1}$
Increment in the D $MinD_{ATP}$ (8X)	128 $\mu m^2 s^{-1}$	16 $\mu m^2 s^{-1}$	0.02 $\mu m^2 s^{-1}$
Increment in the D $MinD_{ADP}$ (8X)	16 $\mu m^2 s^{-1}$	128 $\mu m^2 s^{-1}$	0.02 $\mu m^2 s^{-1}$
Increment in the D $MinD^m$ (8X)	16 $\mu m^2 s^{-1}$	16 $\mu m^2 s^{-1}$	0.16 $\mu m^2 s^{-1}$
Increment in the D $MinD_{ATP}$ and $MinD_{ADP}$ (2X)	32 $\mu m^2 s^{-1}$	32 $\mu m^2 s^{-1}$	0.02 $\mu m^2 s^{-1}$
Increment in the D $MinD_{ADP}$ and $MinD^m$ (2X)	16 $\mu m^2 s^{-1}$	32 $\mu m^2 s^{-1}$	0.04 $\mu m^2 s^{-1}$
Increment in the D $MinD_{ATP}$ and $MinD^m$ (2X)	32 $\mu m^2 s^{-1}$	16 $\mu m^2 s^{-1}$	0.04 $\mu m^2 s^{-1}$
Increment in the D $MinD_{ATP}$ and $MinD_{ADP}$ (4X)	64 $\mu m^2 s^{-1}$	64 $\mu m^2 s^{-1}$	0.02 $\mu m^2 s^{-1}$
Increment in the D $MinD_{ADP}$ and $MinD^m$ (4X)	16 $\mu m^2 s^{-1}$	64 $\mu m^2 s^{-1}$	0.08 $\mu m^2 s^{-1}$
Increment in the D $MinD_{ATP}$ and $MinD^m$ (4X)	64 $\mu m^2 s^{-1}$	16 $\mu m^2 s^{-1}$	0.08 $\mu m^2 s^{-1}$
Increment in the D $MinD_{ATP}$ and $MinD_{ADP}$ (8X)	128 $\mu m^2 s^{-1}$	128 $\mu m^2 s^{-1}$	0.02 $\mu m^2 s^{-1}$
Increment in the D $MinD_{ADP}$ and $MinD^m$ (8X)	16 $\mu m^2 s^{-1}$	128 $\mu m^2 s^{-1}$	0.16 $\mu m^2 s^{-1}$
Increment in the D $MinD_{ATP}$ and $MinD^m$ (8X)	128 $\mu m^2 s^{-1}$	16 $\mu m^2 s^{-1}$	0.16 $\mu m^2 s^{-1}$
Increment in all MinD (2X)	32 $\mu m^2 s^{-1}$	32 $\mu m^2 s^{-1}$	0.04$\mu m^2 s^{-1}$
Increment in all MinD (4X)	64 $\mu m^2 s^{-1}$	64 $\mu m^2 s^{-1}$	0.08 $\mu m^2 s^{-1}$
Increment in all MinD (8X)	128 $\mu m^2 s^{-1}$	128 $\mu m^2 s^{-1}$	0.16 $\mu m^2 s^{-1}$

Table 3 Diffusion coefficient (D) of $MinD_{ATP}$, $MinD_{ADP}$ and $MinD^m$ modification

3.4.3 Modification of the reaction rate k1, k2, k3 and k4

The reaction rates of k1, k2, k3 and k4 were simulated according to Table 4. Modification was made based on increment of two folds (2X), four folds (4X) and eight folds (8X).

Reaction Rate	k1	k2	k3*	k4
k value from established model	0.022 $\mu m\ s^{-1}$	0.03 $\mu m^3\ s^{-1}$	*7 s^{-1}	5 s^{-1}
Increment in the k1 (2X)	0.044 $\mu m\ s^{-1}$	0.03 $\mu m^3\ s^{-1}$	7 s^{-1}	5 s^{-1}
Increment in the k1 (4X)	0.088 $\mu m\ s^{-1}$	0.03 $\mu m^3\ s^{-1}$	7 s^{-1}	5 s^{-1}
Increment in the k1 (8X)	0.176 $\mu m\ s^{-1}$	0.03 $\mu m^3\ s^{-1}$	7 s^{-1}	5 s^{-1}
Increment in the k2 (2X)	0.022 $\mu m\ s^{-1}$	0.06 $\mu m^3\ s^{-1}$	7 s^{-1}	5 s^{-1}
Increment in the k2 (4X)	0.022 $\mu m\ s^{-1}$	0.12 $\mu m^3\ s^{-1}$	7 s^{-1}	5 s^{-1}
Increment in the k2 (8X)	0.022 $\mu m\ s^{-1}$	0.24 $\mu m^3\ s^{-1}$	7 s^{-1}	5 s^{-1}
Increment in the k3 (2X)	0.022 $\mu m\ s^{-1}$	0.03 $\mu m^3\ s^{-1}$	14 s^{-1}	5 s^{-1}
Increment in the k3 (4X)	0.022 $\mu m\ s^{-1}$	0.03 $\mu m^3\ s^{-1}$	28 s^{-1}	5 s^{-1}
Increment in the k3 (8X)	0.022 $\mu m\ s^{-1}$	0.03 $\mu m^3\ s^{-1}$	56 s^{-1}	5 s^{-1}
Increment in the k4 (2X)	0.022 $\mu m\ s^{-1}$	0.03 $\mu m^3\ s^{-1}$	7 s^{-1}	10 s^{-1}
Increment in the k4 (4X)	0.022 $\mu m\ s^{-1}$	0.03 $\mu m^3\ s^{-1}$	7 s^{-1}	20 s^{-1}
Increment in the k4 (8X)	0.022 $\mu m\ s^{-1}$	0.03 $\mu m^3\ s^{-1}$	7 s^{-1}	40 s^{-1}
Increment in the k1 and k2 (2X)	0.044 $\mu m\ s^{-1}$	0.06 $\mu m^3\ s^{-1}$	7 s^{-1}	5 s^{-1}
Increment in the k1 and k2 (4X)	0.088 $\mu m\ s^{-1}$	0.12 $\mu m^3\ s^{-1}$	7 s^{-1}	5 s^{-1}
Increment in the k1 and k2 (8X)	0.176 $\mu m\ s^{-1}$	0.24 $\mu m^3\ s^{-1}$	7 s^{-1}	5 s^{-1}
Increment in the k1 and k3 (2X)	0.044 $\mu m\ s^{-1}$	0.03 $\mu m^3\ s$	14 s^{-1}	5 s^{-1}
Increment in the k1 and k3 (4X)	0.088 $\mu m\ s^{-1}$	0.03 $\mu m^3\ s$	28 s^{-1}	5 s^{-1}
Increment in the k1 and k3 (8X)	0.176 $\mu m\ s^{-1}$	0.03 $\mu m^3\ s$	56 s^{-1}	5 s^{-1}
Increment in the k1 and k4 (2X)	0.044 $\mu m\ s^{-1}$	0.03 $\mu m^3\ s$	7 s^{-1}	10 s^{-1}
Increment in the k1 and k4 (4X)	0.088 $\mu m\ s^{-1}$	0.03 $\mu m^3\ s$	7 s^{-1}	20 s^{-1}
Increment in the k1 and k4 (8X)	0.176 $\mu m\ s^{-1}$	0.03 $\mu m^3\ s$	7 s^{-1}	40 s^{-1}
Increment in the k2 and k3 (2X)	0.022 $\mu m\ s^{-1}$	0.06 $\mu m^3\ s^{-1}$	14 s^{-1}	5 s^{-1}
Increment in the k2 and k3 (4X)	0.022 $\mu m\ s^{-1}$	0.12 $\mu m^3\ s^{-1}$	28 s^{-1}	5 s^{-1}
Increment in the k2 and k3 (8X)	0.022 $\mu m\ s^{-1}$	0.24 $\mu m^3\ s^{-1}$	56 s^{-1}	5 s^{-1}

Reaction Rate	k1	k2	k3*	k4
Increment in the k2 and k4 (2X)	0.022 $\mu m\ s^{-1}$	0.06 $\mu m^3\ s^{-1}$	7 s^{-1}	10 s^{-1}
Increment in the k2 and k4 (4X)	0.022 $\mu m\ s^{-1}$	0.12 $\mu m^3\ s^{-1}$	7 s^{-1}	20 s^{-1}
Increment in the k2 and k4 (8X)	0.022 $\mu m\ s^{-1}$	0.24 $\mu m^3\ s^{-1}$	7 s^{-1}	40 s^{-1}
Increment in the k3 and k4 (2X)	0.022 $\mu m\ s^{-1}$	0.03 μm^3 s	14 s^{-1}	10 s^{-1}
Increment in the k3 and k4 (4X)	0.022 $\mu m\ s^{-1}$	0.03 μm^3 s	28 s^{-1}	20 s^{-1}
Increment in the k3 and k4 (8X)	0.022 $\mu m\ s^{-1}$	0.03 μm^3 s	56 s^{-1}	40 s^{-1}
Increment in the k1, k2 and k3 (2X)	0.044 $\mu m\ s^{-1}$	0.06 $\mu m^3\ s^{-1}$	14 s^{-1}	5 s^{-1}
Increment in the k1, k2 and k3 (4X)	0.088 $\mu m\ s^{-1}$	0.12 $\mu m^3\ s^{-1}$	28 s^{-1}	5 s^{-1}
Increment in the k1, k2 and k3 (8X)	0.176 $\mu m\ s^{-1}$	0.24 $\mu m^3\ s^{-1}$	56 s^{-1}	5 s^{-1}
Increment in the k1, k2 and k4 (2X)	0.044 $\mu m\ s^{-1}$	0.06 $\mu m^3\ s^{-1}$	7 s^{-1}	10 s^{-1}
Increment in the k1, k2 and k4 (4X)	0.088 $\mu m\ s^{-1}$	0.12 $\mu m^3\ s^{-1}$	7 s^{-1}	20 s^{-1}
Increment in the k1, k2 and k4 (8X)	0.176 $\mu m\ s^{-1}$	0.24 $\mu m^3\ s^{-1}$	7 s^{-1}	40 s^{-1}
Increment in the k1, k3 and k4 (2X)	0.044 $\mu m\ s^{-1}$	0.03 μm^3 s	14 s^{-1}	10 s^{-1}
Increment in the k1, k3 and k4 (4X)	0.088 $\mu m\ s^{-1}$	0.03 μm^3 s	28 s^{-1}	20 s^{-1}
Increment in the k1, k3 and k4 (8X)	0.176 $\mu m\ s^{-1}$	0.03 μm^3 s	56 s^{-1}	40 s^{-1}
Increment in the k1, k2, k3 and k4 (2X)	0.044 $\mu m\ s^{-1}$	0.06 $\mu m^3\ s^{-1}$	14 s^{-1}	10 s^{-1}
Increment in the k1, k2, k3 and k4 (4X)	0.088 $\mu m\ s^{-1}$	0.12 $\mu m^3\ s^{-1}$	28 s^{-1}	20 s^{-1}
Increment in the k1, k2, k3 and k4 (8X)	0.176 $\mu m\ s^{-1}$	0.24 $\mu m^3\ s^{-1}$	56 s^{-1}	40 s^{-1}

Table 4 Reaction rate of k1, k2, k3 and k4 modification

CHAPTER 4

RESULT

4.1 Optimization of the reaction and diffusion rate

Several lines of evidence indicated that the dynamic cellular distribution of MinD and MinE were independent. This was approved by laboratory experiment by B. Shen and J. Lutkenhaus, (2010) in their FtsZ-I374V strain when there is no minicell production in the population that is lack in MinE. The new suggested model were based on the MinDE only with discarded MinE in the system to equally imitate the environment of *in vivo* experiment.

4.2 Modification of the initial value of $MinD_{ATP}$, $MinD_{ADP}$ and $MinD^{m}$ molecules

Modification of initial value $MinD_{ATP}$, $MinD_{ADP}$ and $MinD^{m}$ molecules was done by increasing the value to two folds, four folds, and eight folds.

In $MinD_{ATP}$, the significant difference can be seen in the production of $MinD_{ADP}$, which was lesser, or almost none in eight folds modification. The simulation period also took longer time in eight folds increment.

In $MinD_{ADP}$, almost the same pattern was observed except the total number of all MinD molecules increased as the initial value of $MinD_{ADP}$ increased in eight folds increment. In term of simulation period, it was observed that eight folds increment took longer time as compare to two folds increment.

In $MinD^{m}$, for two folds increment, it was observed that the production of all MinD were at the same level. However, comparison between two folds and eight folds cannot be done as the eight folds increment was too large for the system to simulate the model.

4.3 Modification of the Diffusion Coefficient of $MinD_{ATP}$, $MinD_{ADP}$ and $MinD^{m}$

The diffusion rate for the MinD at cytoplasm also played a critical role in MinD membrane association activity. Any significant changes to the diffusion rate will caused a long period of simulation time. Here, we increased the diffusion rate for all three species of MinD; $MinD_{ATP}$, $MinD_{ADP}$ and $MinD^{m}$. The increment was set to two folds, four folds and eight folds.

In $MinD_{ATP}$, almost the same pattern was observed between two folds and eight folds modification. However, exception can be made in production of $MinD^{m}$, where there was a significant reduction of the molecules mentioned. The simulation time period was longer in eight folds modification.

Similar to $MinD_{ATP}$, $MinD_{ADP}$ also produced almost the same pattern. The production of all MinD however, stay at the same level though at eight folds modification the simulation period took longer time.

In $MinD^{m}$, significant reduction was observed in both two folds and eight folds modification. The same pattern was observed in both. However, as predicted, the simulation period was longer for eight folds modification.

Changes in combination of two modified MinD also was done. Significant reduction can be seen in eight folds increment. The eight folds increment took a longer simulation period.

In $MinD_{ATP}$ and $MinD^{m}$ modification, similar pattern was observed in both two folds and eight folds models. Significant reduction in $MinD^{m}$ molecules was observed. The eight folds increment took a longer simulation period.

In $MinD_{ADP}$ and $MinD^{m}$ modification, similar pattern was observed in both two folds and eight folds models. Significant reduction in $MinD^{m}$ molecules was observed. The eight folds increment took a longer simulation period.

Through naked eyes observation, the production of $MinD^{m}$ molecules in modification for all MinD for two folds increment seems to localize more at the poles rather than at the septum compare to eight folds model. However, the oscillation observed in both models did not restrict the $MinD^{m}$ molecules to the poles. This result suggested that there is a possibility for MinD to localize at the poles with further optimization.

4.4 Modification of the reaction rate k1, k2, k3 and k4

The modification of reaction rate k1, k2, k3, and k4 were done according to two folds, four folds and eight folds increment to observed the effect of reaction rate in MinD localization. The conditions were as follow; a) modification in k1 rate, b) modification in k2 rate, c) modification in k3 rate, d) modification in k4 rate, e) modification in k1 and k2 rates, f) modification in k1 and k3 rates, g) modification in k1 and k4 rates, h) modification in k2 and k3 rates, i) modification in k2 and k4 rates, j) modification in k3 and k4 rates, k) modification in k1, k2 and k3 rates, l) modification in k1, k2 and k4 rates, m)modification in k1, k3 and k4 rates, n) modification in k2, k3 and k4 rates, o) modification in k1, k2, k3 and k4 rates.

In the modification of the first reaction, $MinD_{ATP} \xrightarrow{k_1} MinD^{m}$ with reaction rate k1, it was observed that almost the same pattern produced in both two folds and eight folds increment. Production of all MinD molecules was almost at the same level. When two folds and eight folds modifications were done to the second reaction

$MinD^m$ + $MinD_{ATP} \xrightarrow{k_2} 2MinD^m$ with reaction rate k2, no particular pattern was observed in all MinD molecules in both models

In third reaction, $MinD^m \xrightarrow{k_3} MinD_{ADP}$ with reaction rate k3 however, shows a different pattern from reaction (1) and reaction (2). The eight folds increment shows an obvious loss of $MinD^m$ molecules compare to two folds increment. Further explanation will be discussed in next chapter.

For the last reaction, $MinD_{ADP} \xrightarrow{k_4} MinD_{ATP}$, the increment of reaction rate k4 in two folds and eight folds resulted in almost the same pattern. Observations were also done in two, three and four modified reaction rate simultaneously.

CHAPTER 5

DISCUSSION

5.1 Discussion

In the rod shape environment that simulates the environment of *E.coli*, it is known that there are high curvatures at the membrane poles compare to the other places in the cell. Due to this phenomenon, when MinD molecules were released from the membrane, the probability for the MinD molecules to rebind back with the membrane is high. Thus, although the MinD molecules tend to move freely along the membrane, collision is more favorable at the region with the highest curvature that will result in the poles localization.

5.2 Initial molecule

There was no oscillation of molecules from pole to pole activity observed in any of the models with modified initial MinD molecules. The removal of MinE from the original model has obviously disrupted the whole MinDE system, thus it is unknown whether the modification of initial value of MinD will affect the new suggested model bypassing MinE system.

5.3 Diffusion rate

Both single and simultaneous modification of diffusion rate showed no particular pattern in $MinD^m$ molecules. The increment of two, four or eight folds did not display any localization of MinD to the poles. Hence, we assumed that the capability of MinD to bind with the membrane at the poles is low with the increment of diffusion rate. Figure 3 shows

the example of simultaneous modification of $MinD_{ATP}$ and $MinD_{ADP}$ at four folds. Although there were some patches produced, $MinD^{m}$ molecules however did not stay long enough at the poles to enable FtsZ inhibition. We assumed that the increment of diffusion rate decreased the rebinding rate for MinD localization at the poles regardless of the high curvature region.

5.4 Reaction rate

5.4.1 Single modification

The simulation show interesting results for modified reaction rate of k3. A single modification of k3 seems to produce patches that nearly restrict the molecules of membrane MinD to the poles. Figure 4 shows the snapshots taken from Spatiocyte. The patches can be clearly seen at t = 900.0s. We assumed that the increment of k3 increased the velocity of $MinD^{m}$ molecules that affecting the binding rate and localization to the poles. Although at a certain time, there was a point where the patches move to the poles, there were not endure long enough to inhibit FtsZ formation.

5.4.2 Simultaneous modification

Although single modification of k3 showed an interesting result, observation that was achieved from simultaneous modifications were not as expected. The patches that were produced from simultaneous simulation did not localize specifically at the poles. Instead, it disperses closely within the membrane.

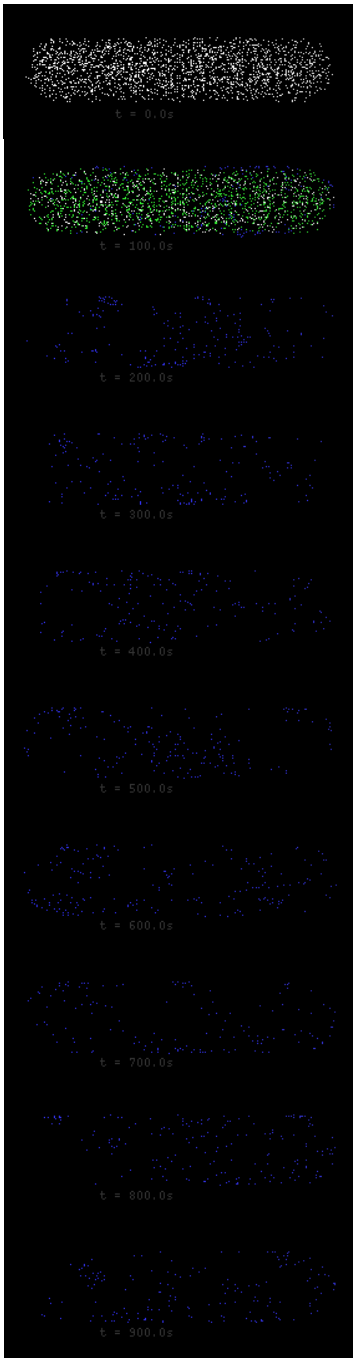

Figure 3 Simultaneous modifications of $MinD_{ATP}$ and $MinD_{ADP}$ at four folds. $MinD_{ATP}$ (white), $MinD_{ADP}$ (green) and $MinD^{m}$ (blue). Noted that other molecules were deliberately disabled to focus on $MinD^{m}$ molecule.

Figure 4 Four folds modification of reaction rate k3.

Arrows shows the patches that nearly localized at both poles at t = 900.0s. $MinD_{ATP}$ (white), $MinD_{ADP}$ (green) and $MinD^{m}$ (blue). Noted that other molecules were deliberately disabled to focus on $MinD^{m}$ molecule.

CHAPTER 6

CONCLUSION

6.1 Conclusion

In this research, investigation on the effects of MinD diffusion-reaction rate to the dynamic oscillation of Min-proteins and description of the differences in MinC/MinD sensitivity between polar and internal Z rings in *Escherichia coli* was done. The main objective of the investigation is to observe the behavior of MinD upon changes to the MinDE model to simulate the new suggested model that bypassing MinE, using spatiocyte, a computational lattice based algorithm application. This research provides important information such as the effect of MinD molecules to any modification in parameter value that involve in the system.

Model from MinDE system suggested by Huang *et. al.* (2003) and further modified and improved by S.N.V. Arjunan and M. Tomita (2009) was applied to optimize the diffusion-reaction rate. Thus, comparison between the results from two models provide a better understanding on the effect of diffusion-reaction rate among Min proteins in the oscillation that eventually will disrupt the filamentation of FtsZ at the poles. The disruption of FtsZ will lead to the formation of Z ring at midcell for binary fusion.

Modification on the diffusion-reaction produced patches pattern in the simulation that eventually disperses within the cell whereby a further optimization needs to be done. Most of the simulation did not display any localization at the poles. However, only one simulation with modification of reaction rate k3 shows a pattern that nearly restricts the $MinD^{m}$ to the poles. The original model of MinDE system that we try to achieve is shown in Figure 5.

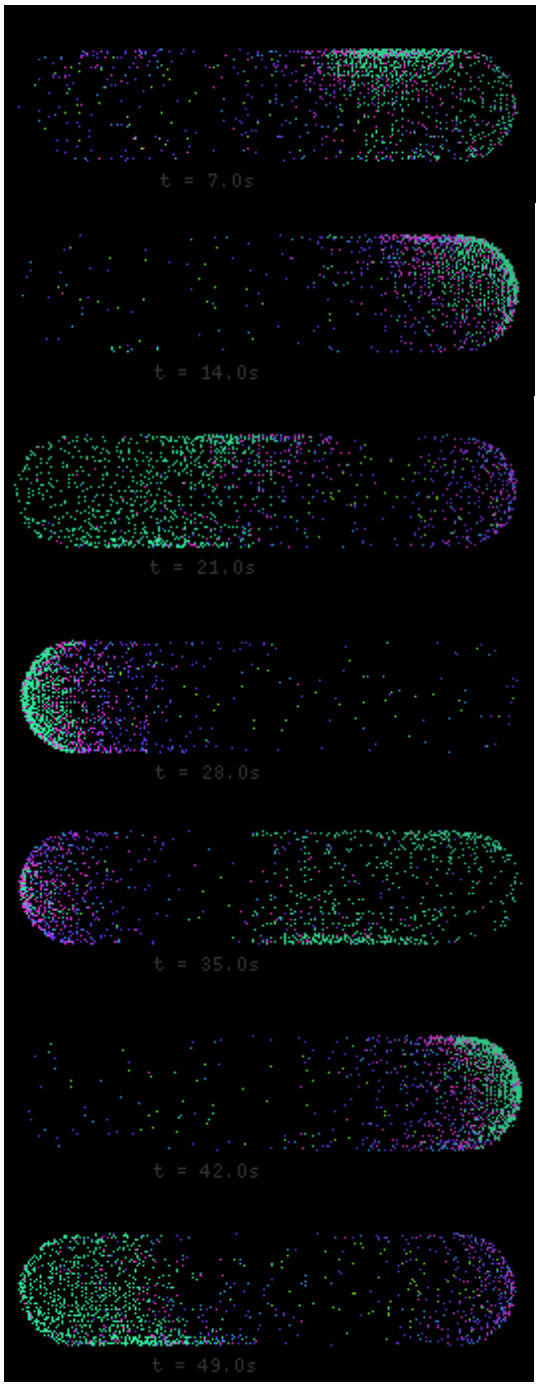

Figure 5 Original model of MinDE System.

Oscillation of $MinD^m$ (turquoise), $MinDE^m$ (blue), $MinE^m$ (purple), with transient membrane attachment of $MinE^m$ according to the reaction based on Arjunan S.N.V and Tomita M. (2009). The new suggested model will omit the MinE molecules.

6.2 Future Work

In order to complete the new suggested model bypassing MinE in the Z ring formation, optimization of diffusion reaction rate need to be done. The investigation will provide information to simulate the model.

Using the latest version of Spatiocyte (v3.2.2) the future work will be carried out in a triangular system that is predicted to provide more sharply curved membrane that enables the patches to localize at poles, hence, facilitate the modification in the actual rod shape environment of *E.coli.*